CHALMERS

Development of Numerical Methods for Accurate and Efficient Scale-Resolving Simulations

MAGNUS CARLSSON

Department of Mechanics and Maritime Sciences
CHALMERS UNIVERSITY OF TECHNOLOGY
Göteborg, Sweden April 2021

THESIS FOR THE DEGREE OF LICENTIATE OF ENGINEERING IN THERMO AND FLUID DYNAMICS

Development of Numerical Methods for Accurate and Efficient Scale-Resolving Simulations

MAGNUS CARLSSON

Department of Mechanics and Maritime Sciences
Division of Fluid Mechanics
CHALMERS UNIVERSITY OF TECHNOLOGY

Göteborg, Sweden April 2021

Development of Numerical Methods for Accurate and Efficient Scale-Resolving Simulations
MAGNUS CARLSSON

Thesis for the degree of Licentiate of Engineering 2021:11
ISSN 1652-8565
Department of Mechanics and Maritime Sciences
Division of Fluid Mechanics
Chalmers University of Technology
SE-412 96 Göteborg
Sweden
Telephone: +46 (0)31-772 1000

Chalmers Reproservice
Göteborg, Sweden April 2021

Development of Numerical Methods for Accurate and Efficient Scale-Resolving Simulations

MAGNUS CARLSSON
Department of Mechanics and Maritime Sciences
Division of Fluid Mechanics
Chalmers University of Technology

Abstract

Hybrid RANS (Reynolds-Averaged Navier-Stokes)-LES (Large-Eddy Simulation) techniques are considered to be sufficiently accurate and computationally affordable for the aeronautical industry. Scale-resolving simulations is a powerful tool that can accurately predict complex unsteady compressible high-Reynolds-number turbulent flows, as often encountered aeronautical applications. However, since the turbulent scales are resolved instead of modeled, higher demand is placed on the underlying numerical methods used in the simulations.

This thesis explores and develops numerical methods suitable for hybrid RANS-LES. The methods are implemented in the Computational Fluid Dynamics (CFD) solver M-Edge, a compressible unstructured node-centered edge-based solver.

A low-dissipative, low-dispersive numerical scheme was calibrated and verified in LES of turbulent channel flow and Decaying Homogeneous Isotropic Turbulent (DHIT). It was shown that numerical dissipation and dispersion needs to be carefully tuned, in order to accurately predict resolved turbulent stresses and the correct decay of turbulent kinetic energy. The reported results are in good agreement with reference DNS and experimental data.

The optimized numerical scheme was then applied to simulate developing hybrid RANS-LES turbulent channel flow. In order to mitigate the grey area region in the LES zone, a Synthetic Turbulence Generator (STG) was applied at the RANS-LES interface. It was shown that using upstream turbulent statistics from a precursor LES or RANS, the recovery length of the skin friction coefficient could be reduced to just a few boundary layer thicknesses.

A new implicit gradient reconstruction scheme suitable for node-centered solvers was proposed. It was shown that the reconstruction scheme achieves fourth-order scaling on regular grids and third-order scaling on irregular grid for an analytical academic case. The Navier-Stokes Characteristic Boundary Condition (NSCBC) was implemented and verified for transport of an analytical vortex. It was shown that special boundary treatment is needed for transporting turbulent structures through the boundary with minimal reflections.

Keywords: Numerical methods, High-order gradient reconstruction, Scale-resolving simulation, Turbulence modelling, Hybrid RANS-LES, Synthetic Turbulence

To my family.

Acknowledgements

I would like to thank my supervisor who gave my the opportunity to pursue a Ph.D.: Lars Davidson at Chalmers, Shia-Hui Peng at FOI and Sebastian Arvidson at Saab Aeronautics. Their support and guidance has been invaluable so far in this work, and I am looking forward working with you for the continuation project.

I would like to thank Peter Eliasson and Per Weinerfelt at Saab Aeronautics for providing support regarding the flow solver M-Edge and for the theoretical input on my work.

I would finally like to thank my friends and family for the support and especially my girlfriend Sara for always encouraging me and putting up with my irrational working hours.

This work has been funded by the Swedish Governmental Agency for Innovation Systems (VINNOVA), the Swedish Defence Materiel Administration (FMV) and the Swedish Armed Forces within the National Aviation Research Programme (NFFP, Contract No. 2017–04887) and Saab Aeronautics. The simulations were performed on resources provided by the Swedish National Infrastructure for Computing (SNIC) at the National Supercomputer Centre (NSC).

Magnus Carlsson
Göteborg, April 2021

NOMENCLATURE

Greek letters

ρ	density
σ_{ij}	viscous stress tensor
μ	dynamic viscosity
ν	kinematic viscosity
Δ	local filter-width
ε	dissipation rate

Roman letters

u_i	i^{th} component of the velocity vector
x_i	i^{th} component of the position vector
p	pressure
e_0	total energy
κ	thermal conductivity
T	temperature
C_P	specific heat at constant pressure
C_V	specific heat at constant volume
R	universal gas constant
γ	heat capacity ratio
P_r	Prandtl number
c	speed of sound
t_{ij}	turbulent stress tensor
k	turbulent kinetic energy

Abbreviations

CFD	Computational Fluid Dynamics
NSCBC	Navier-Stokes Characteristic Boundary Condition
RANS	Reynolds Averaged Navier-Stokes
LES	Large Eddy Simulation
ELES	Embedded LES
DNS	Direct Numerical Simulation
HRLM	Hybrid RANS-LES Modeling
STG	Synthetic Turbulence Generator
SEM	Synthetic Eddy Method
(D)DES	(Delayed) Detached Eddy Simulation

Thesis

This thesis consists of an extended summary and the following appended papers:

Paper A M. Carlsson, L. Davidson, S.H. Peng, and S. Arvidson. "Parametric Investigation of Low-dissipation Low-dispersion Schemes for Unstructured Flow Solvers in Large Eddy Simulation". *2020 AIAA SciTech*. 2020

Paper B M. Carlsson, L. Davidson, S.H. Peng, and S. Arvidson. *Investigation of Turbulence Injection Methods in Compressible Flow Solvers in Large Eddy Simulation*. Chalmers University of Technology, Göteborg, Sweden, Technical Report, 2021

Paper C M. Carlsson, L. Davidson, S.H. Peng, and S. Arvidson. *Higher Order Gradients on Unstructured Meshes using Compact Formulation for Node-Centered Schemes*. Chalmers University of Technology, Göteborg, Sweden, Technical Report, 2021

Paper D M. Carlsson, L. Davidson, S.H. Peng, and S. Arvidson. *Implementation of Nonreflecting Inlet and Outlet Boundary Conditions in the Subsonic Regime for a Node-Based Compressible Solver*. Chalmers University of Technology, Göteborg, Sweden, Technical Report, 2021

Contents

Part I
Extended Summary

The scope of this thesis is the development of numerical methods used in hybrid RANS-LES modeling. A low-dissipative, low-dispersive numerical scheme is evaluated in paper A, where it is calibrated and verified in LES of turbulent channel flow and Decaying Homogeneous Isotropic Turbulent (DHIT). It was concluded in the work reported that numerical dissipation needs to be carefully reduced, in order to accurately resolve relevant turbulent scales while still achieving a converged solution. The predictions are further improved by the enhanced dispersive properties of the scheme.

In paper B, an embedded hybrid RANS-LES approach is verified using a synthetic turbulence generator (STG), the Synthetic Eddy Method (SEM), in order to introduce turbulent fluctuations into a LES domain. Two different methods to inject the synthetic fluctuation into the LES domain was investigated. It was concluded that introducing synthetic fluctuations at the RANS-LES interface can effectively mitigate the grey-area region for turbulent channel flow.

In order to further increase the numerical accuracy of the flow solver, a new implicit gradient reconstruction scheme was proposed in paper C. The reconstruction scheme achieves fourth-order scaling on regular grids and third-order scaling on irregular grid for an analytical academic case. As future work, the new gradient scheme is planned to be implemented into the compressible flow solver M-Edge.

From the work in paper B, it was concluded that special attention to the boundary conditions is needed. To avoid nonphysical reflections in scale-resolving simulations, the boundaries of a truncated flow domain needs to be able to handle incoming and outgoing numerical or physical waves. The Navier-Stokes Characteristic Boundary Condition (NSCBC) was implemented and verified for transporting an analytical vortex through the boundaries in paper D.

This thesis is organized as follows. An introduction is given Chapter 1 where hybrid RANS-LES methods are introduced with an aeronautical perspective. A survey of turbulent inflow boundary conditions is given, along with numerical methods commonly used in hybrid RANS-LES. The numerical methods used in this thesis are presented in Chapter 2. Chapter 3 further validates the numerical method used for two additional test cases, subsonic flow over 2 D periodic hills and supersonic flow over a cylindrical base. Finally, Chapter 4 summarizes the outcomes of the thesis work and the proposed continuation of the work.

Chapter 1
Introduction

The aerospace industry needs to reduce their product development and life cycle costs, reduce the environmental footprint related to the products and increase the product capability and availability to meet costumers' and consumers' requirements. By introducing flow simulations techniques which are able to accurately simulate complex unsteady compressible flows, there is a great potential to reduce costs for wind tunnel and flights tests. Moreover, with an increased usage of model-based design and advanced flow simulations, there are strong possibilities to introduce multi-disciplinary simulations and optimization techniques, which potentially leads to novel and innovative aeronautical products in line with e.g. ACARE 2020 [18] and FlightPath 2050 [20].

To meet the requirements on more cost effective aeronautical products with enhanced capabilities and reduced environmental footprint, improved flow simulation techniques are needed. With improved flow simulation techniques accurate predictions of complex unsteady fluid flows, such as separated flows which e.g. can generate noise, leading to engine disturbances and structural fatigue, can be made. Hybrid RANS (Reynolds-Averaged Navier-Stokes)-LES (Large-Eddy Simulation) techniques are considered to be sufficiently accurate and computationally affordable for the aeronautical industry. Industrially adapted hybrid RANS-LES modelling (HRLM) techniques thus have the potential to improve product quality, give a more efficient design process with shorter time-to-market for new products and products with a reduced environmental impact. Moreover, HRLM techniques have a great potential to complement or replace wind tunnel and flight tests.

The methods used today for aerodynamics design are mainly based on steady-state RANS simulations, which often provide reliable results for steady flows and attached boundary layers. More accurate and reliable turbulence models, based on turbulence-resolving methods, as well as improved numerical schemes need to be introduced into an industrial environment. However, advances in RANS modeling alone are unlikely to alleviate this problem, while the use of LES methods remain unfeasible for various applications for the foreseeable future. Conclusions form the the NASA CFD Vision 2030 [52] document states that Hybrid RANS-LES and wall-modeled LES offers the best prospects for overcoming these problems.

1.1 Hybrid RANS-LES Modeling

Common practices for CFD-based workflows utilize steady RANS although HRLM are increasingly common for certain classes of simulations in which swirling and intentionally separated flows are dominant, such as combustors. The key feature of HRLM is the RANS-type behavior in the vicinity of a solid boundary and a LES-type behavior joint with the RANS-modelled wall layer. In the HRLM framework, the most commonly used methods includes the family of detached eddy simulation (DES) [56, 61, 58], which was extended by boundary-layer shielding, e.g. delayed DES (DDES) [55] and further wall

modelling improvements in the improved DDES (IDDES) [50]. Another family of HRLM includes the partially integrated transport modeling (PITM) method [49, 10], the partially averaged Navier-Stokes (PANS) method [22, 21], and the scale adaptive simulation (SAS) [37]. These models are expected to naturally transition from RANS to LES. Other HRLM are for example the algebraic HYB0-model [42, 40].

In embedded LES (ELES) or "zonal" approaches a user defined LES zone, embedded in the RANS region, is introduced for capturing regions of the flow of particular interest. The aim is to increase accuracy and to reduce the computational effort needed compared to non-zonal approaches. If there is no explicit forcing at the RANS-LES interface, there may occur a delayed transition region where the turbulence is neither modeled or resolved. This so-called "grey area problem" has been extensively studied, see e.g. [2].

1.2 Turbulent Inflow Boundary Conditions

The "grey area problem" can be mitigated by introducing explicitly forced turbulence based on the statistics of the incoming modeled RANS turbulence. The most general approach is to synthesize artificial turbulence based on turbulent length scales and time scales from the mean RANS flow field using a so-called synthetic turbulence generator (STG). An ideal STG should be able to inject turbulent structures that are realistic for the specific problem under study. This involves satisfying the desired mean velocity profile, Reynolds stress tensor, turbulent kinetic energy spectrum, and correct phase information [13].

Common STG methods are e.g. Fourier reconstruction techniques [4, 51], where Fourier series is used as a mean to introduce a spatial correlation. A time filter can be applied to introduce temporal correlation [12]. Another family of approaches is the Synthetic Eddy methods (SEM) [29, 30], where the turbulent field is superimposed by virtual vortical structures. These vortical structures or eddies are randomly generated and convected through a fictional domain giving both spatial and temporal correlation to the fluctuations, which are allowed to induce perturbations to cells in their neighbourhood. Further improvement was made to the original SEM, where it was extended to give a divergence-free (DF-SEM)[43] fluctuating velocity field.

1.3 Numerical Accuracy

Proper resolution of the LES mode in HRLM requires a minimal dissipative and minimal dispersion numerical scheme. In scale-resolving flows, the accuracy and order of the numerical method dictates the capabilities of resolving relevant length and time scales for turbulent flows, where higher-order methods (above second-order) are popular. Higher-order methods can be achieved by increasing the discretization stencil by using additional neighbor points or by assuming a high-order polynomial for each cell. For complex geometries, which are typical for problems in the aeronautical industry, unstructured grids are often used to provide a quick discreization of the flow domain. For an unstructured flow solver, managing this type of grids pose a severe challenge where the cells can have arbitrary shape and number of neighbours. Examples of higher-order methods

for unstructured grids are higher-order finite-volume [33, 1], discontinuous galerkin [11], spectral volume [63, 64] or spectral difference [34, 35]. However, an existing second-order industrially capable flow solver is used, and incorporating the changes needed for these higher order methods would require large changes to the flow solver.

A low-dissipative finite-volume scheme suitable for unstructured compressible solvers was developed by Probst et. al [45], where the added numerical dissipation was effectively reduced and demonstrated for wall-bounded scale resolving flow. To further improve the capabilities of the numerical scheme, a low-dissipation and low-dispersion (LD2) scheme was formulated by Löwe et al. [36, 46], where a higher order extrapolation of the face fluxes is used to control and reduce the numerical dispersion errors.

1.4 Motivation and Objective

This thesis is motivated by the needs for improved simulation accuracy and increased computational efficiency for complex turbulent flows present in aeronautical applications. Even though hybrid RANS-LES simulation have been used for the past two decades, the joint behavior of numerical schemes, synthetic turbulence injection and modeling techniques is still a challenging task that needs special attention in order to increase the simulation robustness and accuracy in industrial applications.

The focus of this thesis is two-fold. The first objective is to explore and assess hybrid RANS-LES turbulence modeling techniques in an industrial framework. The second objective is to further extend and improve the capabilities of an industrially used second-order RANS code to the hybrid RANS-LES regime.

Chapter 2
Modeling and Simulation Methodology

This chapter introduces the governing equations for turbulent flows. These are the modeled variant of the Navier-Stokes equations, which are solved for in Direct Numerical Simulations (DNS). The equations need to be filtered in order to reduce the spatial and temporal resolution requirements, in order to make scale-resolving simulations more accessible to the industry. The Navier-Stokes and its filtered version are presented, along with the turbulence modelling methods used in this thesis. A description of the CFD solver then follows, with a detailed outline of the relevant numerical methods used for scale-resolving simulations.

2.1 Governing Equations

The governing equations for unsteady, compressible flow are the Navier-Stokes equations

$$\frac{\partial \rho}{\partial t} + \frac{\partial (\rho u_i)}{\partial x_i} = 0 \tag{2.1}$$

$$\frac{\partial (\rho u_i)}{\partial t} + \frac{\partial (\rho u_i u_j)}{\partial x_j} = -\frac{\partial p}{\partial x_i} + \frac{\partial \sigma_{ij}}{\partial x_j} \tag{2.2}$$

$$\frac{\partial (\rho e_0)}{\partial t} + \frac{\partial (\rho e_0 u_j)}{\partial x_j} = -\frac{\partial (p u_j)}{\partial x_j} + \frac{\partial}{\partial x_j}\left[\kappa \frac{\partial T}{\partial x_j} + u_i \sigma_{ij}\right] \tag{2.3}$$

where the thermal conductivity κ is set to $\kappa = C_p \mu / P_r$, and the total energy is computed as $e_0 = e + u_i u_i / 2$. For a perfect gas we have $e = C_V T$, $C_V = R/(\gamma - 1)$, $\gamma = C_P / C_V$ and the equation of state is computed as

$$p = (\gamma - 1)\left[\rho e_0 - \frac{1}{2}\rho u_i u_i\right] \tag{2.4}$$

A Newtonian fluid is assumed where the viscous stress tensor is modeled as

$$\sigma_{ij} = \mu \left(\frac{\partial u_i}{\partial x_j} + \frac{\partial u_j}{\partial x_i} - \frac{2}{3}\frac{\partial u_k}{\partial x_k}\delta_{ij} \right) \tag{2.5}$$

where μ is the dynamic molecular viscosity. To solve this set of equations (2.1)-(2.3) in DNS, all relevant spatial and temporal scales in the flow field needs to be resolved. This means that the grid needs to be fine enough to resolve features on the order of the Kolmogorov length scale

$$\eta = (\nu^3 / \varepsilon)^{\frac{1}{4}} \tag{2.6}$$

where ν is the kinematic viscosity and ε is the dissipation rate. Likewise, the time step needs to be fine enough to resolve temporal dynamics on the order of the Kolmogorov time scale

$$\tau = (\nu / \varepsilon)^{\frac{1}{2}} \tag{2.7}$$

These two resolution requirements are impossible today to achieve for industrial flows at high Reynolds numbers. Limitations on available computational resources mean that DNS will not be practical for industry relevant flow cases for the foreseeable future. The aforementioned filtering process of the Navier-Stokes Equations (2.1) - (2.3) reduces the resolution requirement at the cost of introducing additional unknown terms. Hence, modeling techniques such as turbulence modeling is needed to close the set of equations.

2.2 Turbulence Modelling

As mentioned in the previous Section, turbulence modeling is necessary due to the unfeasible computational requirements of DNS for flows of engineering interest. This is achieved by filtering the Navier-Stokes equations. The filtering process reduces the spatial and temporal resolution requirements by introducing additional modeling parameters. The filtering process and the filtered Navier-Stokes solved in the CFD solver used in this thesis are outlined below.

The RANS equations are dervied by using time-averaging, which can for an arbitrary quantity Φ be expressed as

$$\overline{\Phi} = \frac{1}{T}\int_T \Phi \mathrm{d}t, \quad \Phi = \overline{\Phi} + \Phi' \tag{2.8}$$

where the instantaneous part Φ is decomposed into a time-averaged part $\overline{\Phi}$ and a fluctuating part Φ'. In LES, one applies a spatial filter instead, this can be expressed for the quantity Φ in 1D as:

$$\overline{\Phi}(x,t) = \frac{1}{\Delta x}\int_{x-0.5\Delta x}^{x+0.5\Delta x} \Phi(\xi,t)d\xi, \quad \Phi = \overline{\Phi} + \Phi' \tag{2.9}$$

Here, $\overline{\Phi}$ corresponds to a large scale (or resolved part) and Φ' corresponds to subfilter-scale fluctuating part. In (2.9), an implicit filter is used through the finite volume discretisation, where the local control volume on the computational grid represents the spatial filter. In addition to the time (2.8) and space (2.9) filters, the compressible Navier-Stokes contains both ordinary and Favré-filtered [19] quantities. The Favré-filter is defined by

$$\widetilde{\Phi} = \frac{\overline{\Phi\rho}}{\overline{\rho}}, \quad \Phi = \widetilde{\Phi} + \Phi'' \tag{2.10}$$

Here, $\bar{(\cdot)}$ means time-averaged quantities when RANS is applied and spatially-averaged quantities when LES is applied. The Favré filtering is denoted by $\tilde{(\cdot)}$.

After filtering, the compressible Navier-Stokes equations ((2.1) - (2.3)) become

$$\frac{\partial\overline{\rho}}{\partial t} + \frac{\partial(\overline{\rho}\tilde{u}_i)}{\partial x_i} = 0 \tag{2.11}$$

$$\frac{\partial\overline{\rho}\tilde{u}_i}{\partial t} + \frac{\partial(\overline{\rho}\tilde{u}_i\tilde{u}_j)}{\partial x_j} = -\frac{\partial\overline{p}}{\partial x_i} - \frac{\partial\mathcal{T}_{ij}}{\partial x_j} \tag{2.12}$$

$$\frac{\partial(\overline{\rho}\tilde{e}_0)}{\partial t} + \frac{\partial(\overline{\rho}\tilde{e}_0\tilde{u}_j)}{\partial x_j} = -\frac{\partial(\overline{p}\tilde{u}_j)}{\partial x_j} + \frac{\partial \mathcal{H}_j}{\partial x_j} \tag{2.13}$$

where $\mathcal{T}_{ij}$ is the total stress tensor $\mathcal{T}_{ij} \equiv \overline{\rho}\tau_{ij} - \tilde{\sigma}_{ij}$, and the sum of heat flux plus work done by viscous stresses are $\mathcal{H}_j = q_j^t + \kappa\partial\tilde{T}/\partial x_j + \mathcal{T}_{ij}\tilde{u}_j$. The Favré-averaged viscous stress tensor is approximated as

$$\tilde{\sigma}_{ij} = \mu\left(\frac{\partial\tilde{u}_i}{\partial x_j} + \frac{\partial\tilde{u}_j}{\partial x_i} - \frac{2}{3}\frac{\partial\tilde{u}_k}{\partial x_k}\delta_{ij}\right) \tag{2.14}$$

The filtered kinetic energy $k \equiv \tau_{ii}/2$ should be included in the expression for total energy $\tilde{e}_0 = e + \tilde{u}_i\tilde{u}_i/2 + k$ due to the filtering process. The equation of state is then given by

$$\overline{p} = (\gamma - 1)\left[\overline{\rho}\tilde{e}_0 - \overline{\rho}\frac{1}{2}\tilde{u}_k\tilde{u}_k - \overline{\rho}k\right] \tag{2.15}$$

The filtering process has introduced two additional unknowns that need to be modeled, the turbulent stresses and the turbulent heat flux

$$\tau_{ij} = \widetilde{u_i u_j} - \tilde{u}_i\tilde{u}_j \tag{2.16}$$

$$q_j^t = -C_P\overline{\rho}\left(\widetilde{u_j T} - \tilde{T}u_j\right) \tag{2.17}$$

A common approach is to use the Boussinesq approximation, where an eddy viscosity μ_t is introduced to relate the turbulent stresses to the mean flow. The assumption is that the turbulent shear stress is proportional to the rate of mean strain

$$\tau_{ij} = -\nu_t\left(\frac{\partial\tilde{u}_i}{\partial x_j} + \frac{\partial\tilde{u}_j}{\partial x_i} - \frac{2}{3}\frac{\partial\tilde{u}_k}{\partial x_k}\delta_{ij}\right) + \frac{2}{3}\delta_{ij}k \tag{2.18}$$

and the turbulent heat flux is modeled as a diffusion term

$$q_j^t = C_P\frac{\mu_t}{Pr_t}\frac{\partial\tilde{T}}{\partial x_j} \tag{2.19}$$

Many different models for ν_t of varying complexity exists in the literature, in the following sections the turbulence models used in this thesis are outlined.

2.2.1 Subgrid Scale Modeling

In LES the large scales of the turbulent spectrum are resolved, whereas as the scales smaller than the local grid resolution are modeled. A popular and simple expression of computing ν_t in (2.18) is the Smagorinsky model [53]

$$\begin{aligned}\nu_{sgs} &= (C_S\Delta)^2|\tilde{S}| \\ |\tilde{S}| &\equiv \sqrt{2\tilde{S}_{ij}\tilde{S}_{ij}}\end{aligned} \tag{2.20}$$

where the local filter-width is taken as the cubic root of local cell volume

$$\Delta = (\delta V_I)^{1/3} \tag{2.21}$$

and the model constant C_S practically takes values ranging from 0.1 to 0.2 depending on the flow. One limiting behavior of this model is the incorrect scaling close to walls. This is usually alleviated by using damping functions that gives the correct near-wall behaviour. However, these damping functions usually requires the distance to the wall and the skin friction as input parameters, possibly leading to complex implementation issues.

The Wall-Adapting Local Eddy-Viscosity (WALE) [14] model addresses this issue by providing a more complex expression in terms of resolved spatial derivatives, that automatically fulfills the near-wall scaling. The subgrid viscosity is defined as

$$\begin{aligned} \nu_t &= (C_m \Delta)^2 \frac{(\mathcal{S}_{ij}^d \mathcal{S}_{ij}^d)^{3/2}}{(\tilde{S}_{ij}\tilde{S}_{ij})^{5/2} + (\mathcal{S}_{ij}^d \mathcal{S}_{ij}^d)^{5/4}} \\ \mathcal{S}_{ij}^d &= \frac{1}{2}\left(\frac{\partial \tilde{u}_i}{\partial x_l}\frac{\partial \tilde{u}_l}{\partial x_j} + \frac{\partial \tilde{u}_j}{\partial x_l}\frac{\partial \tilde{u}_l}{\partial x_i}\right) - \frac{1}{3}\frac{\partial \tilde{u}_m}{\partial x_l}\frac{\partial \tilde{u}_l}{\partial x_m}\delta_{ij} \end{aligned} \tag{2.22}$$

A common value for the model constant for wall bounded flow is $C_m = 0.325$ [14].

2.2.2 Hybrid RANS-LES Modeling

Hybrid RANS-LES methods have been developed for the past 20 years, where the idea is to utilise the best aspects of RANS and LES approaches. The hybrid methods produces RANS-type behavior in the vicinity of a solid boundary, where RANS models have successively proven to accurately model attached boundary layers using a moderately coarse mesh. The HRLM switches to LES mode in off-wall regions and in region with separated flow, where LES models have proven to be able to effectively predict transient flow features.

Several methods are available in the literature, where the most well-known is the Detached Eddy Simulation (DES) [57, 61, 55, 50] family of models. Two different hybrid methods are used throughout this thesis, a DES version of the one-equation Spalart-Allmaras (SA) turbulence model and an algebraic zero-equation HRLM (HYB0 [42, 40]).

2.2.3 S-A DDES

The one-eqaution model of Spalart and Allmaras was especially developed for applications of aerodynamic flows and is empirically built as follows [54]

$$\frac{\partial \tilde{\nu}}{\partial t} + \frac{\partial(\tilde{\nu}\tilde{u}_j)}{\partial x_j} = C_{b1}\tilde{\nu}\tilde{S} + \frac{1}{\sigma}\left[\frac{\partial}{\partial x_j}\left((\tilde{\nu}+\nu)\frac{\partial \tilde{\nu}}{\partial x_j}\right) + C_{b2}\frac{\partial \tilde{\nu}}{\partial x_j}\frac{\partial \tilde{\nu}}{\partial x_j}\right] - C_{w1}f_w\frac{\tilde{\nu}^2}{d_w^2} \tag{2.23}$$

where the quantities on the right hand side correspond to production, diffusion and destruction. The quantity $\tilde{S}$ corresponds to a modified vorticity and d_w is the wall

distance. The other parameters are coefficients or blending functions defined in the original paper [54]. The turbulent eddy viscosity is computed from $\tilde{\nu}$ by $\nu_t = \tilde{\nu} f_{\nu 1}$, where $f_{\nu 1}$ is given as a function of the ratio $\chi = \tilde{\nu}/\nu$.

The SA-DES [57] model is based on the RANS model given in Eq. (2.23), where the wall distance d_w is replaced by

$$\tilde{d} = \min(d_w, C_{DES}\Delta) \tag{2.24}$$

where

$$\Delta = \max(\Delta_x, \Delta_y, \Delta_z) \tag{2.25}$$

and $C_{DES} = 0.65$ is a modeling constant calibrated in simulations of decaying isotropic turbulence. In the near wall region the model reduces to the S-A RANS model $\tilde{d} = d_w$, whereas far away from the wall, $d_w \gg \Delta$ leading to $\tilde{d} = C_{DES}\Delta$ and the model acts as a subgrid scale model. The formulation of the length scale (2.24) caused premature switching from RANS to LES. This grid-induced separation [55] is caused by the DES model extending the LES region into the boundary layer, where the grid is not fine enough to resolve the turbulent stresses. This problem was addressed in the Delayed DES version of the model, where the DES-length scale (2.24) was redefined as

$$\tilde{d} = d_w - f_d \max(0, d_w - C_{DES}\Delta) \tag{2.26}$$

where f_d is a shielding function which takes on the value unity in the LES region and zero elsewhere. This model has been applied to various flow configurations such as the backward facing step, circular cylinder, airfoils and rudimentary landing gear [55, 48].

2.2.4 HYB0

The HYB0 [42, 40] model uses a mixing length model in the near-wall RANS region combined with the Smagorisnky model (2.20) in the off-wall LES region. In the RANS region the eddy viscosity is modeled as

$$\tilde{\mu}_t = \overline{\rho}\tilde{l}_\mu^2 |\tilde{S}| \tag{2.27}$$

where the length scale $\tilde{l}_\mu$ is proportional to the wall distance d_w, reading $\tilde{l}_\mu = f_\mu \kappa d_w$ and $\kappa = 0.418$ is the von Kármán constant. The near-wall behavior is controlled by the empirical damping function f_μ given by

$$f_\mu = \tanh\left(\frac{R_t^{1/3}}{2.5}\right) \tag{2.28}$$

where $R_t = \tilde{\mu}_t/\mu$. In the off-wall LES region, the subgrid turbulent viscosity reads

$$\mu_{sgs} = \rho(C_S\Delta)^2 |\tilde{S}| \tag{2.29}$$

with $C_S = 0.12$ and $\Delta = \sqrt{(\Delta_{max}^2 + \delta V^{2/3})/2}$, where δV is the volume of local control volume and Δ_{max} is given by (2.25). The switch between RANS and LES modes is

achieved by modifying the RANS turbulent length scale over the RANS-LES interface into $l_\mu = f_s \tilde{l}_\mu$ so that $\mu_t = \overline{\rho} l_\mu^2 |\tilde{S}|$ in the RANS region. The empirical matching function reads

$$f_s = \frac{1}{2}\left[\exp\left(-\frac{R_s^{0.75}}{4.75}\right) + \exp\left(-\frac{R_s^{0.3}}{2.5}\right)\right] \tag{2.30}$$

where $R_s = \tilde{\mu}_t / \mu_{sgs}$ is the ratio between the intensities of the RANS and LES turbulence. The use of f_s gives a smooth transition for the RANS-LES interface. The hybrid viscosity is then computed by

$$\mu_h = \begin{cases} \mu_t, & \text{if} \tilde{l}_\mu < \Delta \\ \mu_{sgs}, & \text{if} \tilde{l}_\mu \geq \Delta \end{cases} \tag{2.31}$$

The HYB0 model has for example been examined in simulations of fundamental turbulent flows, including wall-bounded flows and separated flow [42], and more complex flow cases such as flow over a rudimentary landing gear [41] and transonic duct flow [3].

2.3 Numerical Methods

The CFD solver used in this thesis is the M-Edge code, which is an edge- and node-based Navier-Stokes flow solver applicable for both structured and unstructured grids [15, 17]. The finite volume discretisation of a node is obtained by applying the integral formulation of the filtered governing equations (2.11)-(2.13) to a control volume surrounding node i,

$$\delta V_i \frac{\partial q_i}{\partial t} + \sum_{j=1}^{n_i} F_{ij} S_{ij} + \sum_{j=1}^{n_i} G_{ij} S_{ij} = \delta V_i Q_i \tag{2.32}$$

where δV_i is the volume surrounding node i, $q_i = (\rho, \rho u, \rho v, \rho w, \rho E)^T$ are the unknown conservative variables in node i, F_{ij} and G_{ij} are the cell face convective and viscous fluxes between nodes i and j, S_{ij} is the cell face area connecting the dual control volumes of the nodes, and Q_i is the source term computed directly at the node. In the following sections the main numerical methods in this thesis are outlined.

2.3.1 Temporal Discretization

For time-accurate unsteady simulations Eq. (2.32) is integrated in time using a second-order backward difference scheme. A dual-time stepping methodology exploiting an explicit low-storage multistage Runge-Kutta scheme [27] is used to advance the solution between physical time steps. The convective, diffusive and source terms (2.32) are lumped into the residual

$$\delta V \frac{\partial q}{\partial t} + R(q) = 0 \tag{2.33}$$

where the physical time derivative is discretized as

$$\frac{\partial q}{\partial t} = \frac{3q^{n+1} - 4q^n + q^n}{2\Delta t} \tag{2.34}$$

where Δt is the physical time step. Equation (2.33) is converted to a steady state problem for each physical time step, where a dual-time derivative is introduced

$$\frac{\partial q^*}{\partial \tau} = -R^*(q^*) \tag{2.35}$$

and a modified residual

$$R^*(q^*) = R(q^*) + \frac{3q^* - 4q^n + q^{n-1}}{2\Delta t} \tag{2.36}$$

The left hand side of Eq.(2.35) is driven to zero and time accuracy according to Eq.(2.34) is achieved when sufficient convergence is reached. A m-stage Runge–Kutta scheme is used for time advancement in dual-time

$$\begin{aligned} q^{(0)} &= q^{(k)} \\ q^{(k,m)} &= q^{(0)} - \alpha_m \frac{\Delta\tau}{\delta V} R^*(q^{(k,m-1)}) \\ &\vdots \\ q^{(k+1)} &= q^{(k,m)} \end{aligned} \tag{2.37}$$

where $\Delta\tau$ is the dual-time step and α_m is the coefficients according to the Runge-Kutta scheme. Convergence is achieved after $k+1$ inner-iterations, $q^{(k+1)} \approx q^{n+1}$, usually that's taken when the residual of (2.35) has dropped two to three orders of magnitude. A three-stage RK scheme is used to solve the steady-state problem, where the coefficients with good smoothing properties are given by [15]

$$\alpha_1 = \frac{2}{3}, \quad \alpha_2 = \frac{2}{3}, \quad \alpha_3 = 1 \tag{2.38}$$

Note that the order of the dual-time stepping scheme with coefficients chosen as Eq. (2.38) is only first-order. However, this does not however degrade the solution quality since accuracy in dual-time for the steady state problem is irrelevant. The convergence of the local time-stepping scheme is accelerated by using implicit residual smoothing and full-approximation storage (FAS) multigrid [27].

2.3.2 Spatial Discretization

The convective fluxes are discretized according to the skew-symmetric energy preserving formulation of Kok [31] together with an artifical matrix dissipation [59]

$$F_{ij} = F\left(\frac{q_L + q_R}{2}\right) - D_{ij}(q) \tag{2.39}$$

where q_L, q_R are higher order extrapolated face values for reducing dispersion errors [36], where the subscripts $_L$ and $_R$ refer to the left (node i) and right (node j) values at the cell face ij. D_{ij} is the artificial viscosity term to be explained below.

The boundary conditions are implemented in a weak formulation, in which a set of temporary flow variables are computed and used in the calculations of the boundary flux added to the residual. The residual then updates all unknown variables including the boundary values [16]. The viscous fluxes are discretized with a second-order central scheme.

Numerical Dissipation

For the present study where unsteady calculations are considered, the underlying numerical method consists of an explicit finite volume second-order centered scheme, augmented with a blending of second- and fourth-order artificial dissipation [28, 59]. The artificial viscosity in Eq. (2.39) is given by Jameson's standard scheme

$$D_{ij}(q) = \left|\frac{\partial F}{\partial q}\right|_{ij} \left[\varepsilon_{ij}^{(2)}(q_i - q_j) - \varepsilon_{ij}^{(4)}(L(q_i) - L(q_j))\right] \tag{2.40}$$

where L is the undivided Laplacian and the convective flux Jacobian $|\frac{\partial F}{\partial q}|_{ij} = R_{ij}|\Lambda|_{ij}R_{ij}^{-1}$ is computed and diagonalized according to Langer [32]. The parameters $\varepsilon_{ij}^{(2)}$ and $\varepsilon_{ij}^{(4)}$ correspond to second- and fourth-order dissipation, respectively. The choice of $\varepsilon_{ij}^{(2)} = 0.5$, $\varepsilon_{ij}^{(4)} = 0$ gives a pure upwind scheme. To reduce the level of dissipation the scaling factors are chosen as

$$\varepsilon_{ij}^{(2)} = \min[\kappa^{(2)} \max(\Psi_i, \Psi_j), 0.5] \tag{2.41}$$

where $\kappa^{(2)}$ is a constant, Ψ_i is a sensor based on the normalized second difference of the pressure given by Eq. (2.43). Other formulations of Eq. (2.41) are given below. $\varepsilon_{ij}^{(4)}$ is taken as the difference between a constant $\kappa^{(4)}$ and $\varepsilon_{ij}^{(2)}$

$$\varepsilon_{ij}^{(4)} = \max[0.0, \kappa^{(4)} - \varepsilon_{ij}^{(2)}] \tag{2.42}$$

such that in presence of shocks the higher differences are switched off in order to prevent oscillations.

Shock Capturing Methods

For high speed flows the flow solver needs to be able to distinguish discontinuities in the flow field. The standard pressure based sensor by Jameson [28]

$$\Psi_i = \frac{|\sum_{k=1}^{m_0}(\tilde{p}_i - \tilde{p}_k)|}{\sum_{k=1}^{m_0}(\tilde{p}_i + \tilde{p}_k)} \tag{2.43}$$

identifies regions with large pressure differences, e.g. shock waves, and return a value close to unity. The numerical scheme is then reduced to a first-order scheme through Eqs. (2.41) and (2.40). This is necessary since according to the work by Godunov [23], any monotonicity preserving numerical scheme in presence of shock waves can be at most first-order accurate. For regions with a smooth continuously varying flow field the

sensor given by Eq. (2.43) is mainly switched off and the scheme follows the fourth-order dissipation in Eq. (2.40).

A different variant of sensor targeted for minimizing excessive dissipation in shock/turbulence interaction in LES was formulated by Ducros [39]. The sensor is a modification to Jameson's sensor and is obtained by multiplying Ψ of Eq. (2.43) with a local function Φ_i defined by

$$\Phi_i = \frac{(\nabla \cdot \mathbf{u})^2}{(\nabla \cdot \mathbf{u})^2 + (\nabla \times \mathbf{u})^2 + \epsilon} \tag{2.44}$$

where the sensor includes the dilation and rotation of the flow field. Hence, regions with resolved turbulence will reduce the added dissipation. The second-order dissipation is then reformulated as

$$\varepsilon_{ij}^{(2)} = \min[\kappa^{(2)} \max(\Psi_i \Phi_i, \Psi_j \Phi_j), 0.5] \tag{2.45}$$

It was shown to effectively distinguish between shocks and compressible turbulence [39]. However, it is not capable of separating large dilatations (shocks) from small dilatational disturbances. Also, in flow regions where vorticity is negligible even very small dilatations will activate the switch. This can add dissipation where it is not wanted and can also introduce spurious oscillations, which both can degrade the accuracy the solution. A modification of the Ducros sensor was presented by Hendrickson et al. [24]

$$\Theta_i = \frac{(\nabla \cdot \mathbf{u})^2}{(\nabla \cdot \mathbf{u})^2 + (\nu \frac{|\mathbf{u}|}{\min l_c})^2 + \epsilon} \tag{2.46}$$

Here, ν is included to control the sensitivty of the switch. In Eq. (2.46) a different frequency scale was chosen instead of the vorticity as in Eq. (2.44). A dimensional analysis yielded the local velocity magnitude $|\mathbf{u}|$ and the local minimum cell dimension, $\min l_c$, as relevant scales, where for small grid spacings, a smaller jump in $|\mathbf{u}|$ is required to appear as a discontinuity. The second-order dissipation is then formulated as

$$\varepsilon_{ij}^{(2)} = \min[\kappa^{(2)} \max(\Theta_i \Phi_i, \Theta_i \Phi_j), 0.5] \tag{2.47}$$

where it was shown to give narrow localised dissipation in presence of shocks [24].

Numerical Dispersion

For the conventional central flux, the values of q_L and q_R are given by the respective nodal values. In the low-dispersion scheme [36], the left and right states are extrapolated from the left and right values by using the gradient of the variables in the nodes,

$$\phi_L = \phi_i + \alpha \nabla \phi_i \cdot d_{ij}, \quad \phi_R = \phi_j - \alpha \nabla \phi_j \cdot d_{ij} \tag{2.48}$$

where ϕ is a scalar, d_{ij} is the distance vector between the two nodes and $\nabla \phi_i, \nabla \phi_j$ are the gradients of ϕ in the two nodes, respectively. The left and right values are then used in the flux given by Eq. (2.39). In this thesis, the gradients are evaluated with a weighted Green-Gauss' approximation. The parameter α can be chosen to reduce the dispersion error for a specific range of wave numbers.

To obtain a fourth-order of the derivative for a finite difference scheme, Taylor expansion shows that one has to choose $\alpha = 1/3$. However, it is possible to show that in a finite volume scheme $\alpha = 1/4$ gives a fourth-order estimation of the face flux. In [36], Löwe et al. investigated the values $\alpha = 0.36$ and $\alpha = 0.4$, which showed better performance in remedy dispersion features on a coarse mesh for an analytical case, while accepting higher dispersion errors on fine meshes compared to $\alpha = 1/3$. They concluded that $\alpha = 0.36$ gave the most favorable cancellation properties [36] and used it in a range of studies [46, 44, 47] for scale-resolving simulations.

2.3.3 Low Mach Number Preconditioning

Low speed preconditioning is introduced to reduce the stiffness for low speed flows where the difference between the speed of sound and local velocity is large. The positive definite preconditioning matrix P is based on Turkel's preconditioning method [62], where it is multiplied with the steady state Equations (2.35)

$$P^{-1}\frac{\partial q^*}{\partial \tau} + R^*(q^*) = 0 \quad \Leftrightarrow \quad \frac{\partial q^*}{\partial \tau} + PR^*(q^*) = 0 \tag{2.49}$$

The preconditioning matrix multiplies the entire residual vector. The basic idea is that it modifies the speed of sound and replaces it with an artificial speed of sound close to the local velocity, thus reducing the stiffness for low speed flows. For time-accurate scale-resolving simulations of low speed flows it is crucial to introduce low speed preconditioning to reduce numerical dissipation, see e.g. [9, 45].

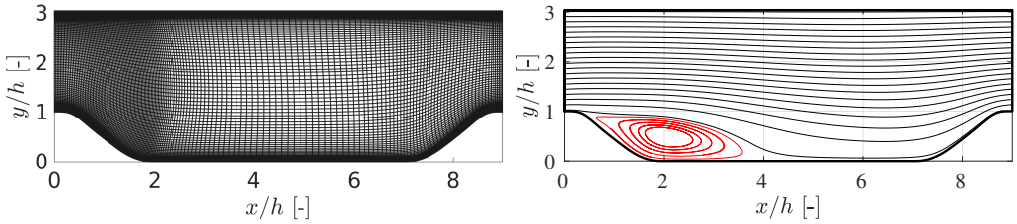

Figure 3.1: *Periodic flow over a 2-D hill: flow domain considered and its dimensions. Computational grid (left) and stream lines for* $Re_h = 10595$ *(right).*

Chapter 3
Implementation and Verification

This chapter summarizes the flow cases used for calibration and evaluation of the methods presented in Chapter 2. The assessment and evaluation of the aforementioned numerical methods of the turbulent channel flow and the DHIT are presented in paper A. The following flow cases are additional results to further verify the numerical methods.

A brief introduction describing the flow case and the results are presented. All simulations have been performed with the unstructured compressible flow solver M-Edge, see section 2.3.

3.1 Periodic Hills

The flow over 2-D hills is a common numerical test case for flow separation with reattachment, streamwise periodicity, alternating adverse and favorable pressure gradient effects, Reynolds-stress anisotropy etc. [5]. The flow configuration is characterized by the Reynolds number based on the hill height h and the mean velocity U_b over the hill crest $Re_h = U_b h/\nu$. Two different Reynolds numbers are considered, $Re_h = 10595$ and $Re_h = 37000$. The computational domain extends $9h$ in streamwise direction, $3h$ in wall normal direction and $4.5h$ in spanwise direction. A grid shown in Fig. 3.1 consisting of $N_x \times N_y \times N_z = 160 \times 80 \times 32$ with uniform spacing in z-direction was used. The same grid was used in the ATAAC project [26]. Hybrid RANS/LES results using the S-A DDES model (2.23) and the HYB0-model (2.27) for different numerical settings are compared to reference LES data [60, 38]. Optimized numerical settings [9] using the LD2 scheme given by Eq. (2.48) are compared with a standard central scheme. The time step for the simulations was set to $\Delta t U_b/h = 1.0 \cdot 10^{-3}$.

Important measures for this flow is the prediction of the recirculation region downstream of the hill, mean velocity profile and resolved Reynolds stresses. First, $Re_h = 10595$ is considered, where qualitative representation of the recirculation region is visualized by the red stream lines in Fig. 3.1. Results averaged in time and in the spanwise directions are presented. The velocity profile of the axial velocity the resolved shear stress component

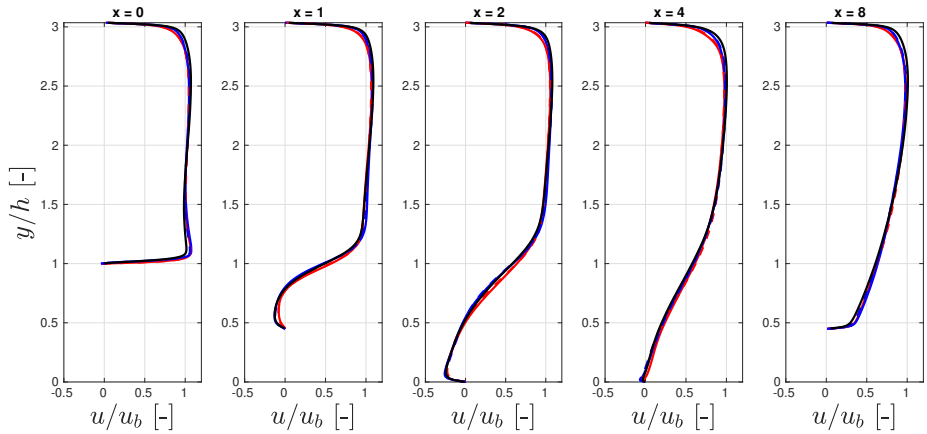

Figure 3.2: *Hybrid RANS/LES of Periodic Hills at* $Re_h = 10595$. *Effects of turbulence model and numerical properties on streamwise velocity u. HYB0 Ref scheme (——), HYB0 LD2 scheme (- - -), SA-DDES Ref scheme (——), SA-DDES LD2 scheme (- - -), Reference LES [60](——).*

at five selected streamwise locations $x/h = 0, 1, 2, 4, 8$ are shown in Figs. 3.2 and 3.3. The mean velocity profile is in general well predicted by the RANS/LES methods for both numerical settings compared to the reference LES, where the curves are visually on top of each other for all x-locations. Larger discrepancies between the models and numerical settings are observed in the shear stress profiles, as shown in Fig. 3.3. At $x/h = 1$, both RANS/LES methods underpredict the shear stress caused by the interaction of the recirculation zone and the curved detached shear layer. The enhanced numerical settings of the LD2 scheme compared to the standard scheme does not seem to improve the prediction. However, further downstream at $x/h = 2$ both RANS/LES methods give accurate shear stress prediction compared to the reference LES. At $x/h = 4$, which is a bit upstream of the reattachement point ($x/h = 4.7$ predicted by the LES), larger discrepancies between RANS/LES model and numerical settings is observed. The SA-DDES model slightly overpredicts the shear stress inside the recirculation region for the reference scheme, but the results are improved using the LD2 scheme. The HYB0-model gives a good prediction for both numerical settings.

The skin friction coefficient along the top and bottom wall is shown in Fig. 3.4, where the reference LES data only included the bottom wall. The SA-DDES model predicts the location of the reattachement point very well, whereas the HYB0-model predicts a slightly shorter separation bubble. In general, the SA-DDES gives close agreement with the reference LES. The HYB0-model gives in general a fairly good prediction, except at the top of the hill crest ($x/h = 0$) where the skin friction coefficient is overpredicted. The zero skin friction coefficient here correspond to a local stagnation region which the HYB0-model fails to predict.

Next, the other Reynolds number ($Re_h = 37000$) is considered. The averaged mean velocity profile of the axial velocity, the resolved shear stress component at the same

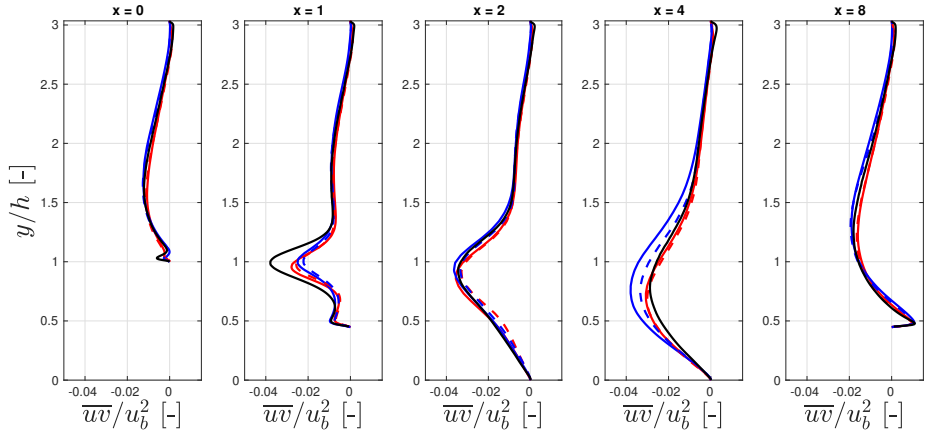

Figure 3.3: *Hybrid RANS/LES of Periodic Hills at* $Re_h = 10595$. *Effects of turbulence model and numerical properties on resolved shear stress* $\overline{u'v'}$. *HYB0 Ref scheme (——), HYB0 LD2 scheme (- - -), SA-DDES Ref scheme (——), SA-DDES LD2 scheme (- - -), Reference LES [60] (——).*

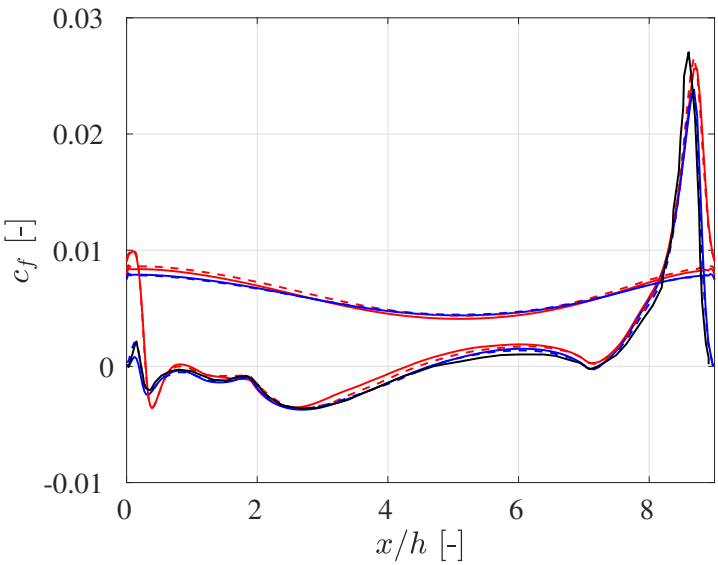

Figure 3.4: *Hybrid RANS/LES of Periodic Hills at* $Re_h = 10595$. *Effects of turbulence model and numerical properties on skin friction coefficient. HYB0 Ref scheme (——), HYB0 LD2 scheme (- - -), SA-DDES Ref scheme (——), SA-DDES LD2 scheme (- - -), Reference LES [60](——).*

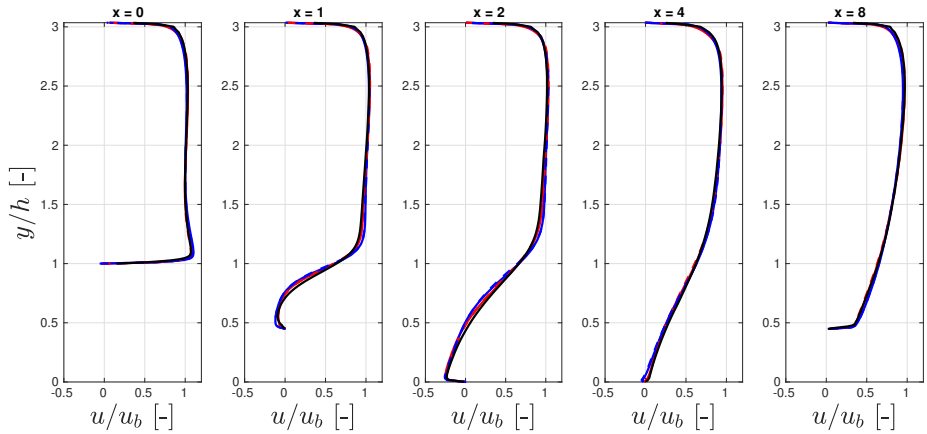

Figure 3.5: *Hybrid RANS/LES of Periodic Hills at* $Re_b = 37000$. *Effects of varying turbulence model and numerical properties on streamwise velocity u. HYB0 Ref scheme (——), HYB0 LD2 scheme (- - -), SA-DDES Ref scheme (——), SA-DDES LD2 scheme (- - -), Reference LES [38] (——).*

streamwise locations and the skin friction coefficient are shown in Figs. 3.5 - 3.6. The profiles of all quantities exhibit qualitatively very similar shape for $Re_h = 37000$ compared to $Re_h = 10595$. The reattachment region appears closer to the hill at $x/h = 3.76$ (reported in [26]) compared to the lower Reynolds number, where this effect is captured slightly better by the HYB0-model compared to the SA-DDES model, as shown in Fig. 3.7. The magnitude of shear stress inside the recirculation region is better captured by the HYB0-model, and also in the post-attachment region at $x/h = 4.0$ as shown in Fig. 3.6. For this case and grid, there are no significant improvements observed with regards to using the LD2 scheme compared to the standard scheme.

3.2 Supersonic Base Flow

A supersonic flow downstream of a blunt-based cylinder is characterized by expansion waves triggered due to the sharp turn of the flow over the base corner. A separation bubble with a low pressure recirculation region contained by a shear layer is formed behind the base. The shear layer undergoes recompression and is reattached at the downstream end of the separation bubble along the axis of symmetry. Due to the recompression, a shock wave is formed. This kind of flow is commonly found behind high speed projectiles, and the low pressure region behind the base can cause drag which can be a major part of the total drag. Thus, the modelling needs to be able to accurately predict the base pressure, along with other relevant properties such as the size of the recirculation bubble and turbulent properties subject to strong compressibilty effects. For this flow, experimental data is available from the study by Herrin and Dutton [25].

The flow is a trailing wake of a circular cylinder with adiabatic walls aligned with a uniform supersonic flow, with a free stream Mach number of $M_\infty = 2.46$. The Reynolds

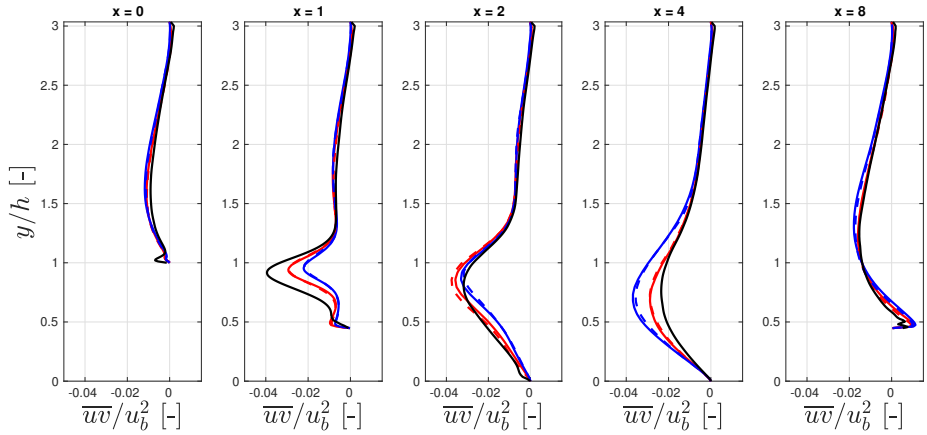

Figure 3.6: *Hybrid RANS/LES of Periodic Hills at* $Re_h = 37000$. *Effects of varying turbulence model and numerical properties on resolved shear stress* $\overline{u'v'}$. *HYB0 Ref scheme (——), HYB0 LD2 scheme (- - -), SA-DDES Ref scheme (——), SA-DDES LD2 scheme (- - -), Reference LES [38] (——).*

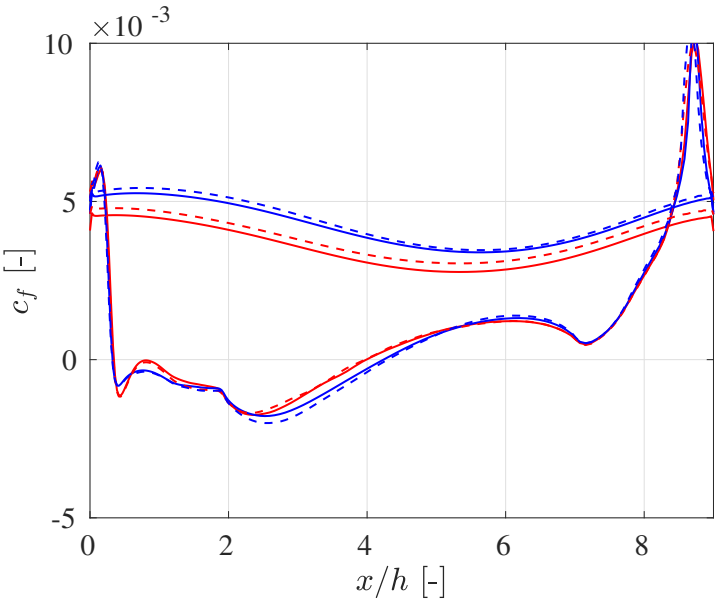

Figure 3.7: *Hybrid RANS/LES of Periodic Hills at* $Re_h = 37000$. *Effects of varying turbulence model and numerical properties on skin friction coefficient. HYB0 Ref scheme (——), HYB0 LD2 scheme (- - -), SA-DDES Ref scheme (——), SA-DDES LD2 scheme (- - -).*

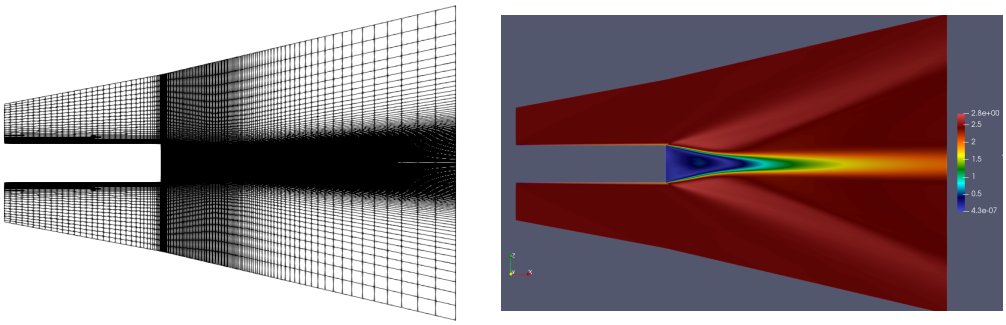

(a) *Grid.* (b) *Mach number contours.*

Figure 3.8: *Case description for supersonic base flow.*

number based on the free stream velocity U_∞, base radius R and free stream viscosity ν is set to $Re_R = 1.632 \cdot 10^6$. A structured mesh containing about 1.8 million nodes is used, see Fig. 3.8a. For this case, the HYB0-model is evaluated along with the spatial schemes and shock capturing methods outlined in Section 2.3.2. A time step of $\Delta t = 0.045R/U_\infty$ is used in the computation. After 5000 time steps, the flow is averaged for 20000 time steps. However, it is observed that the mean flow is still slightly asymmetric after time averaging, which is diminished by further averaging the solution over the azimuthal direction ϕ.

Time and azimuthally averaged flow properties are shown in Figure 3.9. Results are shown for the standard central scheme with Jameson's sensor (2.43), the LD2 scheme with Ducros' sensor (2.44) and the LD2 scheme with Hendrickson's switch (2.46). The purpose of including the switches by Ducros and Hendrickson was to investigate the reduced numerical dissipation due to the inclusion of the resolved vorticity in the formulation for both sensors.

The base pressure is in general well captured for the different numerical settings, whereas the size of the recirculation bubble is a bit overpredicted. The prediction of the shear stress in the shear layer is underpredicted by around 50% at $x/R = 1.57$, which partly occur inside the recirculation bubble. The lowering of numerical dissipation and improved dispersive properties of the LD2 scheme does not seem to improve the prediction of the shear stress in this region. It is believed that a much finer grid is needed to resolve the shear layer turbulence. However, it is encouraging that the combination of the LD2 scheme with a broader stencil than the standard central scheme, combined with the shock capturing methods by Ducros or Hendrickson, does not detoriate the solution outside the recirculation bubble, with the presence of the expansion and compression waves.

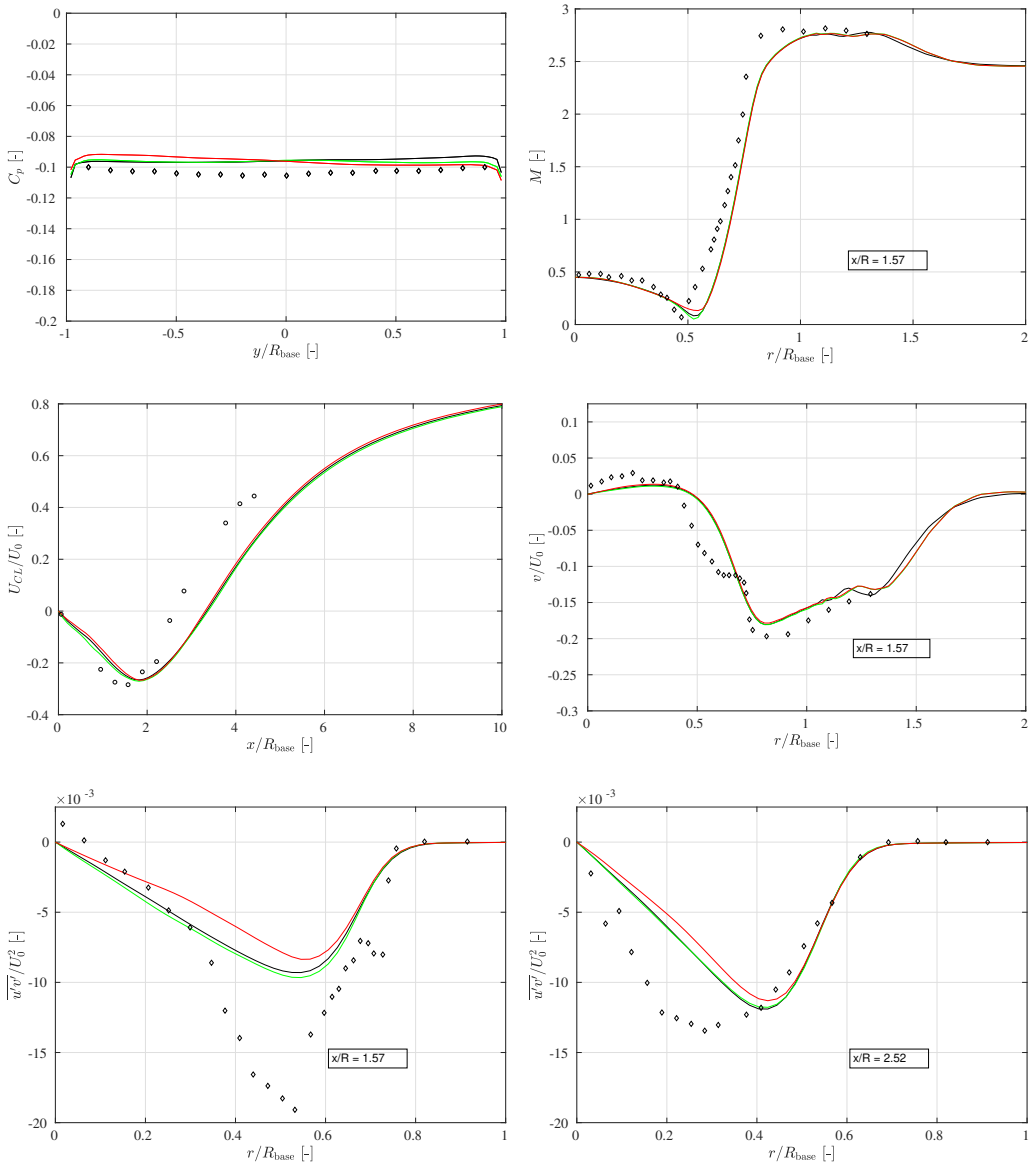

Figure 3.9: *Hybrid RANS/LES of Supersonic Base Flow. Effect of numerical scheme on HYB0 prediction of the ϕ-averaged mean flow. Reference scheme (——), LD2 Ducros switch (——), LD2 Hendrickson switch (——), Experiment [25] (◇).*

Chapter 4
Conclusions and Outlook

This chapter summarizes the work done in the thesis and in the appended papers. Comments are also given on the proposed continuation of the work.

4.1 Summary and Conclusions

A low-dissipative low-dispersive scheme (LD2) by Löwe et al. has been investigated in in order to reduce the dissipative and dispersive numerical errors connected to the convective term. The scheme controls added artificial dissipation through a matrix dissipation operator and can be adapted to low speed flows with a low Mach number preconditioner. The scheme exploits a higher order central reconstruction of the face fluxes to reduce the dispersive numerical error. The numerical scheme was applied in LES of turbulent channel flow and the decaying homogeneous isotropic turbulence (DHIT) for calibration purposes. Additional hybrid RANS-LES of flow over periodic hills and supersonic flow over a cylindrical base further verifies the scheme and give good agreement with reference data.

A sensitivity study on the implementation of the Synthetic-Eddy Method (SEM) to inject synthetic turbulence at the RANS-LES interface in order to mitigate the grey-area problem in the LES region has been made. Two methods have been implemented, where the synthetic turbulent fluctuations is numerically represented by means of, respectively, a volumetric source term or a virtual flux term, where the two methods were implemented through imposing the fluctuations (in the form of a source term or a flux term) at the inlet boundary or in a plane further downstream of the inlet boundary. The methods have been verified in LES of a spatially decaying isotropic turbulence case and a turbulent channel flow.

An implicit least squares gradient (ILSQ) reconstruction scheme with a compact formulation has been derived. A detailed study of two-dimensional gradient calculation for node-centered unstructured data on regular and highly irregular grids has been made. Compared to a standard compact LSQ scheme, which uses only nearest neighbours in the stencil, the implicit scheme also includes information from neighbouring gradients, leading to a linear system to be solved. This allows the assumed polynomial or Taylor expansion in the least squares approach to be of higher order. In this study, a third-order polynomial is assumed for the ILSQ scheme. The ILSQ shows a third-order scaling on highly irregular quadrilateral elements and triangular elements with large variation in number of nearest neighbours. On regular grids, favorable error cancellation allows a fourth-order scaling.

The Navier-Stokes characteristic boundary conditions (NSCBC) has been implemented and evaluated in order to reduce numerical and physical wave reflections from simulation boundaries. The implementation was assessed by the transport of an analytical vortex in the subsonic regime. The current implementation of the boundary condition give satisfactory results for a subsonic outlet, where the vortex is effectively transported

with minimal reflections. For a subsonic inlet, the implementation deviates from results reported in the literature and will be further examined.

The numerical scheme, the synthetic turbulence generator, and the characteristic boundary conditions were implemented and evaluated in M-Edge, a node-centered second-order unstructured compressible finite-volume Navier-Stokes solver. The new gradients scheme was implemented in a stand-alone script, where an implementation of the gradient scheme in the aforementioned flow solver is planned.

4.2 Outlook

The work presented in this thesis and in the appended papers is by no means considered, by the author, finished. The numerical scheme will be further assessed for additional hybrid RANS-LES flow cases. The performance of the numerical scheme will be examined and evaluated on true unstructured grids, which often is encountered in industrial applications of complex aeronautical flow cases.

The implementation of the characteristic boundary conditions needs to be further explored in the next step work. The combination of the synthetic turbulent inlet boundary condition and the characteristic boundary condition is of special interest. The ability to inject synthetic turbulence while not producing unwanted pressure waves and reflections will be examined.

The current study of the new gradient scheme is planned to be followed up by an implementation in a compressible finite-volume flow solver, where the accuracy, feasibility and robustness will be further evaluated on relevant flow cases. If time permits, the gradient scheme will be extended to three dimensions and applied to scale-resolving simulations for hybrid RANS-LES applications.

Chapter 5
Division of work

5.1 Paper A

M. Carlsson, L. Davidson, S.H. Peng, and S. Arvidson. "Parametric Investigation of Low-dissipation Low-dispersion Schemes for Unstructured Flow Solvers in Large Eddy Simulation". *2020 AIAA SciTech*. 2020

The simulations, analysis, post-processing and writing of the paper was done by Carlsson. Davidson, Peng and Arvidson provided support and feedback in the writing process.

5.2 Paper B

M. Carlsson, L. Davidson, S.H. Peng, and S. Arvidson. *Investigation of Turbulence Injection Methods in Compressible Flow Solvers in Large Eddy Simulation*. Chalmers University of Technology, Göteborg, Sweden, Technical Report, 2021

The implementation of the synthetic turbulence generator was performed by Carlsson. Simulations, analysis, post-processing and writing of the paper was done by Carlsson. Davidson, Peng and Arvidson provided support and feedback in the writing process.

5.3 Paper C

M. Carlsson, L. Davidson, S.H. Peng, and S. Arvidson. *Higher Order Gradients on Unstructured Meshes using Compact Formulation for Node-Centered Schemes*. Chalmers University of Technology, Göteborg, Sweden, Technical Report, 2021

The development of the method was done by Carlsson, with theoretical support from Peng. The implementation of the method, simulations, analysis and post-processing was done by Carlsson. Davidson, Peng and Arvidson provided support and feedback in the writing process.

5.4 Paper D

M. Carlsson, L. Davidson, S.H. Peng, and S. Arvidson. *Implementation of Nonreflecting Inlet and Outlet Boundary Conditions in the Subsonic Regime for a Node-Based Compressible Solver*. Chalmers University of Technology, Göteborg, Sweden, Technical Report, 2021

The implementation of the non-reflective boundary conditions was performed by Carlsson. All simulations, analysis, post-processing of results and writing of the paper was done by

Carlsson. Davidson, Peng and Arvidson provided support and feedback in the writing process.

References

[1] R. Abgrall. On Essentially Non-oscillatory Schemes on Unstructured Meshes: Analysis and Implementation. *Journal of Computational Physics* **114**.1 (1994), 45–58. ISSN: 0021-9991. DOI: https://doi.org/10.1006/jcph.1994.1148. URL: https://www.sciencedirect.com/science/article/pii/S002199918471148X.

[2] S. Arvidson, L. Davidson, and S.-H. Peng. Interface methods for grey-area mitigation in turbulence-resolving hybrid RANS-LES. *International Journal of Heat and Fluid Flow* **73** (2018), 236–257. ISSN: 0142-727X. DOI: https://doi.org/10.1016/j.ijheatfluidflow.2018.08.005. URL: https://www.sciencedirect.com/science/article/pii/S0142727X18301656.

[3] S. Arvidson, S.-H Peng, and L. Davidson. Feasibility of Hybrid RANS-LES Modeling of Shock/Boundary-Layer Interaction in a Duct. *Notes on Numerical Fluid Mechanics and Multidisciplinary Design* **117** (Jan. 2012), 245–256. DOI: 10.1007/978-3-642-31818-4_21.

[4] P. Batten, U. Goldberg, and S. Chakravarthy. Interfacing Statistical Turbulence Closures with Large-Eddy Simulation. *AIAA Journal* **42**.3 (2004), 485–492. DOI: 10.2514/1.3496.

[5] M. Breuer, N. Peller, Ch. Rapp, and M. Manhart. Flow over periodic hills – Numerical and experimental study in a wide range of Reynolds numbers. *Computers Fluids* **38**.2 (2009), 433–457. ISSN: 0045-7930. DOI: https://doi.org/10.1016/j.compfluid.2008.05.002. URL: https://www.sciencedirect.com/science/article/pii/S0045793008001126.

[6] M. Carlsson, L. Davidson, S.H. Peng, and S. Arvidson. *Higher Order Gradients on Unstructured Meshes using Compact Formulation for Node-Centered Schemes*. Chalmers University of Technology, Göteborg, Sweden, Technical Report, 2021.

[7] M. Carlsson, L. Davidson, S.H. Peng, and S. Arvidson. *Implementation of Non-reflecting Inlet and Outlet Boundary Conditions in the Subsonic Regime for a Node-Based Compressible Solver*. Chalmers University of Technology, Göteborg, Sweden, Technical Report, 2021.

[8] M. Carlsson, L. Davidson, S.H. Peng, and S. Arvidson. *Investigation of Turbulence Injection Methods in Compressible Flow Solvers in Large Eddy Simulation*. Chalmers University of Technology, Göteborg, Sweden, Technical Report, 2021.

[9] M. Carlsson, L. Davidson, S.H. Peng, and S. Arvidson. "Parametric Investigation of Low-dissipation Low-dispersion Schemes for Unstructured Flow Solvers in Large Eddy Simulation". *2020 AIAA SciTech*. 2020.

[10] B. Chaouat and R. Schiestel. Progress in subgrid-scale transport modelling for continuous hybrid non-zonal RANS/LES simulations. *International Journal of Heat and Fluid Flow* **30**.4 (2009), 602–616. ISSN: 0142-727X. DOI: https://doi.org/10.1016/j.ijheatfluidflow.2009.02.021. URL: https://www.sciencedirect.com/science/article/pii/S0142727X09000551.

[11] B. Cockburn and C.-W. Shu. TVB Runge-Kutta Local Projection Discontinuous Galerkin Finite Element Method for Conservation Laws II: General Framework.

Mathematics of Computation **52**.186 (1989), 411–435. ISSN: 00255718, 10886842. URL: http://www.jstor.org/stable/2008474.

[12] L. Davidson and M. Billson. Hybrid LES-RANS using synthesized turbulent fluctuations for forcing in the interface region. *International Journal of Heat and Fluid Flow* **27** (2006), 1028–1042.

[13] Nitin S. Dhamankar, Gregory A. Blaisdell, and Anastasios S. Lyrintzis. Overview of Turbulent Inflow Boundary Conditions for Large-Eddy Simulations. *AIAA Journal* **56**.4 (2018), 1317–1334. DOI: 10.2514/1.J055528.

[14] F. Ducros, F. Nicoud, and T. Poinsot. "Wall-adapting local eddy-viscosity models for simulations in complex geometries". *Conference on numerical methods for fluid dynamics*. 1998, pp. 293–299.

[15] P. Eliasson. "Edge, a Navier–Stokes solver for unstructured grids". *Finite Volumes for Complex Applications*. Vol. III. CP849. 2002, pp. 527–534.

[16] P. Eliasson, S. Eriksson, and J. Nordström. The influence of weak and strong solid wall boundary conditions on the convergence to steady-state of the navier-stokes equations. *AIAA Paper* 2009-3551 (2009).

[17] P. Eliasson and P. Weinerfelt. "Recent applications of the flow solver Edge". *7th Asian CFD Conference*. CP849. 2007.

[18] *European Aviation: A vision for 2020*. https://www.acare4europe.org/sites/acare4europe.org/file Accessed: August 2020.

[19] A. Favré. "Problems of Hydrodynammics and Continuum Mechanics". *Society for Industrial and Applied Mathematics*. 1969, pp. 231–266.

[20] *Flightpath 2050, Europe's Vision for Aviation*. https://ec.europa.eu/transport/sites/transport/fi Accessed: October 2020.

[21] S. S. Girimaji. Partially-Averaged Navier-Stokes Model for Turbulence: A Reynolds-Averaged Navier-Stokes to Direct Numerical Simulation Bridging Method. *Journal of Applied Mechanics* **73**.3 (Nov. 2005), 413–421.

[22] *PANS Turbulence Model for Seamless Transition Between RANS and LES: Fixed-Point Analysis and Preliminary Results*. Vol. Volume 2: Symposia, Parts A, B, and C. Fluids Engineering Division Summer Meeting. July 2003, pp. 1901–1909.

[23] S. K. Godunov and I. Bohachevsky. Finite difference method for numerical computation of discontinuous solutions of the equations of fluid dynamics. *Matematičeskij sbornik* **47(89)**.3 (1959), 271–306. URL: https://hal.archives-ouvertes.fr/hal-01620642.

[24] T. R. Hendrickson, A. Kartha, and G. V. Candler. "An Improved Ducros Sensor for the Simulation of Compressible Flows with Shocks". *2018 Fluid Dynamics Conference*. DOI: 10.2514/6.2018-3710. eprint: https://arc.aiaa.org/doi/pdf/10.2514/6.2018-3710. URL: https://arc.aiaa.org/doi/abs/10.2514/6.2018-3710.

[25] J. L. Herrin and J. C. Dutton. Supersonic base flow experiments in the near wake of a cylindrical afterbody. *AIAA Journal* **32**.1 (1994), 77–83. DOI: 10.2514/3.11953.

[26] S. Jakirlic. *Extended excerpt related to the test case: flow over a periodical arrangement of 2D hills. Tech. Rep. (2012)*. 2012.

[27] A. Jameson. Time-dependent calculations using multigrid with applications to unsteady flows past airfoils and wings. *AIAA Paper* 91-1596 (1991).

[28] A. Jameson, W. Schmidt, and E. Turkel. "Numerical solution of the Euler equations by finite volume methods using Runge Kutta time stepping schemes". *14th Fluid and Plasma Dynamics Conference*. DOI: 10.2514/6.1981-1259. eprint: https://arc.aiaa.org/doi/pdf/10.2514/6.1981-1259. URL: https://arc.aiaa.org/doi/abs/10.2514/6.1981-1259.

[29] N. Jarrin, S. Benhamadouche, D. Laurance, and R. Prosser. A synthetic-eddy-method for generating inflow conditions for large-eddy simulations. *International Journal of Heat and Fluid Flow* **27** (2006), 585–593.

[30] N. Jarrin, R. Prosser, J.-C. Uribe, S. Benhamadouche, and D. Laurance. Reconstruction of turbulent fluctuations for hybrid RANS/LES simulations using a Synthetic-Eddy Method. *International Journal of Heat and Fluid Flow* **30** (2009), 435–442.

[31] J. C. Kok. A high-order low-dispersion symmetry-preserving finite volume method for compressible flow on curvilinear grids. *Journal of Computational Physics* **228** (2009), 6811–6832.

[32] S. Langer. Investigations of a compressible second order finite volume code towards the incompressible limit. *Computer and Fluids* **149** (2017), 119–137.

[33] X.-D. Liu, S. Osher, and T. Chan. Weighted Essentially Non-oscillatory Schemes. *Journal of Computational Physics* **115**.1 (1994), 200–212. ISSN: 0021-9991. DOI: https://doi.org/10.1006/jcph.1994.1187. URL: https://www.sciencedirect.com/science/article/pii/S0021999184711879.

[34] Y. Liu, M. Vinokur, and Z. J. Wang. "Discontinuous Spectral Difference Method for Conservation Laws on Unstructured Grids". *Computational Fluid Dynamics 2004*. Ed. by C. Groth and D. W. Zingg. Berlin, Heidelberg: Springer Berlin Heidelberg, 2006, pp. 449–454.

[35] G. Lodato, P. Castonguay, and A. Jameson. Structural Wall-modeled LES Using a High-order Spectral Difference Scheme for Unstructured Meshes. *Flow, Turbulence and Combustion* **92**.1-2 (Jan. 2014). WOS:000328844400028, 579–606. DOI: 10.1007/s10494-013-9523-3. URL: https://hal.archives-ouvertes.fr/hal-01612397.

[36] J. Löwe, A. Probst, T. Knopp, and R. Kessler. Low-Dissipation Low-Dispersion Second-Order Scheme for Unstructured Finite-Volume Flow Solvers. *AIAA Journal* **54** (2016). DOI: 10.2514/1.J054956.

[37] Florian M. and Yury E. "A Scale Adaptive Simulation Model using Two-Equation Models". *43rd AIAA Aerospace Sciences Meeting and Exhibit*. DOI: 10.2514/6.2005-1095. eprint: https://arc.aiaa.org/doi/pdf/10.2514/6.2005-1095. URL: https://arc.aiaa.org/doi/abs/10.2514/6.2005-1095.

[38] M. Manhart, C. Rapp, N. Peller, M. Breuer, O. Aybay, Jordan A. Denev, and C. J. Falconi. "Assessment of eddy resolving techniques for the flow over periodically arranged hills up to Re=37,000". *Quality and Reliability of Large-Eddy Simulations II*. Dordrecht: Springer Netherlands, 2011, pp. 361–370.

[39] F. Nicoud and F. Ducros. Subgrid-scale stress modelling based on the square of the velocity gradient tensor. *Flow, Turbulence and Combustion* **63** (1999), 183–200.

[40] S. H. Peng. "Algebraic Hybrid RANS-LES Modelling Applied to Incompressible and Compressible Turbulent Flows". Vol. 4. June 2006. DOI: 10.2514/6.2006-3910.

[41] S. H. Peng. "Hybrid RANS-LES Computations of Turbulent Flow over Rudimentary Landing Gear". June 2013. DOI: 10.2514/6.2013-2913.

[42] S. H. Peng. Hybrid RANS-LES modeling based on zero- and one-equation models for turbulent flow simulation. *4th International Symposium on Turbulence and Shear Flow Phenomena* **3** (Jan. 2005), 1159–1164.

[43] R. Poletto, A. Revell, T. Craft, and N. Jarrin. Divergence free synthetic eddy method for embedded LES inflow boundary conditions. *Seventh international Symposium On Turbulence and Shear Flow Phenomena (TSFP-7)* (2011).

[44] A. Probst. "Scale-Resolving Simulations on Unstructured Meshes with a Low-Dissipation Low-Dispersion Scheme". *New Results in Numerical and Experimental Fluid Mechanics XI*. Cham: Springer International Publishing, 2018, pp. 489–498.

[45] A. Probst and S. Reuß. "Scale-Resolving Simulations of Wall-Bounded Flows with an Unstructured Compressible Flow Solver". *Progress in Hybrid RANS-LES Modelling*. Vol. 130. Springer, 2015, pp. 481–491.

[46] S. Probst, T. Knopp, D. Francois, C. Grabe, T. Landa, and R. Radespiel. Scale-resolving simulations of the streamwise sortex downstream of a delta wing. *AIAA Journal* **54** (2016). DOI: 10.2514/1.J054957.

[47] S. Probst, T. Knopp, D. Francois, C. Grabe, T. Landa, and R. Radespiel. "Scale-resolving Simulations of the Streamwise Vortex Downstream of a Delta Wing". *AIAA Scitech 2019 Forum*. 2019. DOI: 10.2514/6.2019-0331. eprint: https://arc.aiaa.org/doi/pdf/10.2514/6.2019-0331. URL: https://arc.aiaa.org/doi/abs/10.2514/6.2019-0331.

[48] Philippe R. S., M. L. Shur, M. Kh. Strelets, and A. K. Travin. Initial noise predictions for rudimentary landing gear. *Journal of Sound and Vibration* **330**.17 (2011), 4180 –4195. DOI: https://doi.org/10.1016/j.jsv.2011.03.012.

[49] R. Schiestel and A. Dejoan. Towards a new partially integrated transport model for coarse grid and unsteady turbulent flow simulation. *Theoretical and Computational Fluid Dynamics* **18(6)** (2005), 443–468. URL: https://hal.archives-ouvertes.fr/hal-00014542.

[50] Mikhail L. Shur, Philippe R. Spalart, Mikhail Kh. Strelets, and Andrey K. Travin. A hybrid RANS-LES approach with delayed-DES and wall-modelled LES capabilities. *International Journal of Heat and Fluid Flow* **29**.6 (2008), 1638 –1649. ISSN: 0142-727X.

[51] M.L. Shur, P.R. Spalart, M.K. Strelets, and A.K. Travin. Synthetic Turbulence Gnerators for RANS-LES Interfaces in Zonal Simulations of Aerodynamic and Aeroacoustic Problems. *Flow, Turbulence and Combustion* **93** (2014), 63–92.

[52] Jeffrey P. Slotnick, A. Khodadoust, J. Alonso, D. Darmofal, W. Gropp, Elizabeth Lurie, and D. Mavriplis. "CFD Vision 2030 Study: A Path to Revolutionary Computational Aerosciences". 2014.

[53] J. Smagorinsky. General circulation experiments with the primitive equations: I. The basic experiment. *Monthly Weather Review* **91**.3 (Mar. 1963), 99–164. DOI: 10.1175/1520-0493(1963)091<0099:GCEWTP>2.3.CO;2.

[54] P. Spalart and S. Allmaras. "A one-equation turbulence model for aerodynamic flows". *30th Aerospace Sciences Meeting and Exhibit*. DOI: 10.2514/6.1992-439.

[55] P. Spalart, S. Deck, M. Shur, K. Squires, M. Strelets, and A. Travin. A New Version of Detached-eddy Simulation, Resistant to Ambiguous Grid Densities. *Theoretical*

and Computational Fluid Dynamics **20** (July 2006), 181–195. DOI: 10.1007/s00162-006-0015-0.

[56] P. Spalart, W-H Jou, M. Strelets, and S. Allmaras. "Comments on the Feasibility of LES for Wings, and on a Hybrid RANS/LES Approach". *Advanced in DNS/LES*. Jan. 1997.

[57] P. Spalart, W-H Jou, M. Strelets, and S. Allmaras. "Comments on the Feasibility of LES for Wings, and on a Hybrid RANS/LES Approach". Jan. 1997, pp. 137–147.

[58] P.R Spalart. Strategies for turbulence modelling and simulations. *International Journal of Heat and Fluid Flow* **21**.3 (2000), 252 –263. DOI: https://doi.org/10.1016/S0142-727X(00)00007-2.

[59] R. C. Swanson and E. Turkel. On the central-difference and upwind schemes. *Journal of Computational Physics* **101** (1992), 292–306.

[60] L. Temmerman and M.A. Leschziner. "Large Eddy Simulation of separatged flow in a streamwise periodic channel construction". *Second International. Symposium on Turbulence and Shear Flow Phenomena, Stockholm, June 27-29*. 2001.

[61] A. Travin, Michael Shur, Michael Strelets, and Philippe Spalart. Detached-Eddy Simulations Past a Circular Cylinder. *Flow Turbulence and Combustion* **63** (Jan. 2000), 293–313. DOI: 10.1023/A:1009901401183.

[62] E. Turkel, R. Radespiel, and N. Kroll. Assessment of preconditioning methods for multidimensional aerodynamics. *Computer and Fluids* **26** (1997), 613–643.

[63] Z.J. Wang. Spectral (Finite) Volume Method for Conservation Laws on Unstructured Grids. Basic Formulation: Basic Formulation. *Journal of Computational Physics* **178**.1 (2002), 210–251. ISSN: 0021-9991. DOI: https://doi.org/10.1006/jcph.2002.7041. URL: https://www.sciencedirect.com/science/article/pii/S0021999102970415.

[64] Z.J. Wang and Yen Liu. Spectral (Finite) Volume Method for Conservation Laws on Unstructured Grids: II. Extension to Two-Dimensional Scalar Equation. *Journal of Computational Physics* **179**.2 (2002), 665–697. ISSN: 0021-9991. DOI: https://doi.org/10.1006/jcph.2002.7082. URL: https://www.sciencedirect.com/science/article/pii/S0021999102970828.